LU-TP 97-29
November 1997

Investigations into the BFKL Mechanism with a Running QCD Coupling

B. Andersson [1], G. Gustafson [2], H. Kharraziha [3]

Department of Theoretical Physics
University of Lund
Sölvegatan 14A
S-223 62 Lund, Sweden

Abstract

We present approximations of varying degree of sophistication to the integral equations for the (gluon) structure functions of a hadron ("the partonic flux factor") in a model valid in the Leading Log Approximation with a running coupling constant. The results are all of the BFKL-type, i.e. a power in the Bjorken variable $x_B^{-\lambda}$ with the parameter λ determined from the size α_0 of the "effective" running coupling $\bar{\alpha} \equiv 3\alpha_s/\pi = \alpha_0/\log(k_\perp^2)$ and varying depending upon the treatment of the transverse momentum pole. We also consider the implications for the transverse momentum ($k_\perp$) fluctuations along the emission chains and we obtain an exponential falloff in the relevant $\kappa \equiv \log(k_\perp^2)$-variable, i.e. an inverse power $(k_\perp^2)^{-(2+\lambda)}$ with the same parameter λ. This is different from the BFKL-result for a fixed coupling, where the distributions are Gaussian in the κ-variable with a width as in a Brownian motion determined by "the length" of the emission chains, i.e. $\log(1/x_B)$. The results are verified by a realistic Monte Carlo simulation and we provide a simple physics motivation for the change.

[1] bo@thep.lu.se
[2] gosta@thep.lu.se
[3] hamid@thep.lu.se

1 Introduction

1.1 The Contents of this Note

In an earlier paper, [1], we have presented the Linked Dipole Chain (LDC) model as a generalization of the well-known CCFM model (for Ciafaloni-Catani-Fiorani-Marchesini), [2], to describe the hadronic structure functions in Deep Inelastic Scattering (DIS) events. We have further in [3] described a set of results from the model. In this note we would like to continue the investigations and in particular *describe the solutions to the equations for the structure functions when a running coupling is introduced.* We will find power-solutions in the Bjorken-variable, i.e. the (gluon) structure function behaves as $x_B^{-\lambda}$ in the same way as for the BFKL-solutions [4] for a fixed coupling.

The power λ is determined by the strength α_0 in the effective running coupling $\bar{\alpha} \equiv 3\alpha_s/\pi = \alpha_0/\ln(k_\perp^2)$ (In a pure Yang-Mills theory we have used the value $\alpha_0 = 12/11$.) and the treatment of the transverse momentum pole, i.e. the small virtualities in our equations. Actually, it will turn out that the equations become unstable in the sense that the value of the parameter λ is sensitive to the approximate treatment of the running coupling in the soft region where $\ln(k_\perp^2)$ is small.

If we introduce a cutoff in the $\ln(k_\perp^2)$-variable we obtain, however, inside a large region, very stable results for an isolated largest eigenvalue λ. One major finding is that the LDC model in itself contains a suppression of the soft region close to the pole of the coupling constant, and thus contributes significantly to this stabilization (This stems from the averaging over the azimuthal angles). Our result is then for the value of the isolated largest power λ that it is about $\lambda \sim (0.3 - 0.4)\alpha_0$ within a realistic cut-off region.

For the transverse momentum dependence of the structure function we will find the asymptotic solution $(\ln(k_\perp^2))^{\alpha_0/\lambda}$. Further, the transverse energy distribution along the chain will not, as for the BFKL case with a constant coupling, be Gaussian in $\log(k_\perp^2)$ with a width determined, as in a Brownian motion, from the "length" of the emission chains, i.e. $\log(1/x_B)$ [5]. Instead it will be a (negative) exponential in $\log(k_\perp^2)$, i.e. it will behave as an inverse power in the transverse momentum $k_\perp^{-2(2+\lambda)}$ with the same λ-value as above. (Note that the Rutherford parton scattering will behave as $k_\perp^{-4}$. The extra factor $k_\perp^{-2\lambda}$ is due to the larger x_B-values needed for higher $k_\perp$.) This is also born out by a Monte Carlo simulation.

It is a well-known property of diffusion equations with a force (in this case stemming from the running coupling which favours small $k_\perp$-values) that there are on the short time scale (for small $\log(1/x_B)$-values) an erratic behaviour, which can easily be mistaken for a stochastic Brownian motion, before the process reaches its long-time stable distribution. Our estimates of the scales in this case unfortunately indicate that the HERA range is too small for a noticeable change to the above-mentioned power behaviour in $k_\perp$.

We will end this note with a set of simple examples to show the way the model interpolates between the DGLAP [6] and the BFKL mechanisms, the

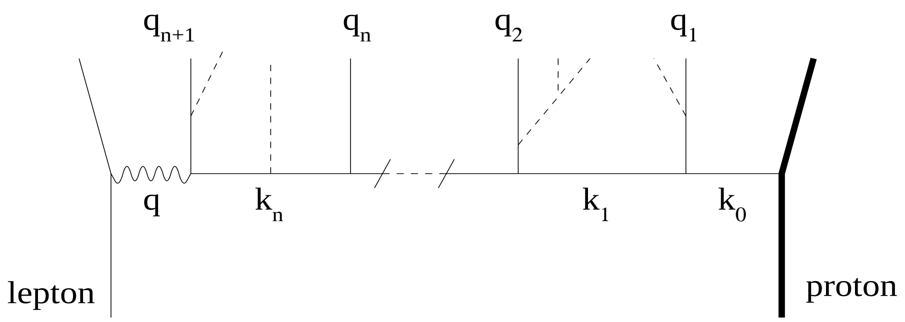

Figure 1: Fan diagram for a DIS event. q_i denote the emitted ISB partons, k_i denote the propagators and the dashed lines are the FSB partons.

reasons why and the mechanisms by which the stable distributions in transverse momentum emerge.

1.2 The CCFM- and the LDC-Models

To introduce the models we note that it is always possible to subdivide the radiation in the states into one part, the Initial State Bremsstrahlung (ISB) (denoted by the vectors q_j in Fig 1) and another part, the Final State Bremsstrahlung (FSB) (the dashed lines in Fig 1). The main requirement is that the FSB partons should be possible to emit in accordance with the QCD coherence conditions and with negligible recoils, if the ISB partons are already emitted. The observable emission weights are given by

$$dw = \sum_I dw^{(0)}(I)\Delta(I) \tag{1}$$

i.e. by the sum over the chosen ISB sets (I) with the basic weight $dw^{(0)}(I)$ to emit these particular partons and a form factor $\Delta(I)$ stemming from the radiative corrections from the choice. To be precise each (I)-state contains a sum over all the exclusive states, containing these ISB partons and any other FSB partons. The FSB should have the property that the corresponding form factors $Sud(F)$ are of the Sudakov type, meaning that, for each fixed (I)-state, the sum over all possible exclusive final states F becomes unity $\sum_F d\omega_I(F)Sud(F) = 1$.

If we ask for a particular value of the observables (Q^2, x_B), i.e. the (squared) "inverse wave-length characteristics of the probe" and the scaled energy-momentum, the Bjorken variable x_B, then we should in Eq (1) sum over the ISB sets, which end on such a configuration.

The choice of the ISB set in the CCFM model is to order all emissions in rapidity (due to the relation between angle and rapidity this means angular ordering, a well-known formulation of the QCD coherence conditions). Then CCFM chose as ISB the emissions with the property that there is no emission further along the rapidity ordering with a larger light-cone energy momentum q_{j+}. The ordering is done from the target-hadron side, i.e. the target is supposed to have a (large) positive light-cone energy-momentum $P \equiv (P_+, P_- \simeq 0, \vec{0}_\perp)$. In the probe-hadron cms the probe (with $-q^2 = Q^2$) has a large energy-momentum along the negative light-cone $q \equiv (-q_+, q_-, \vec{0}_\perp)$. This choice of the ISB is then consistent with QCD coherence but not with the fact that there should be symmetry between the hadron and the probe directions, [7].

Assuming that the recoils can be neglected, the ISB partons with momenta q_j are on their mass shells. Energy-momentum conservation at every ISB vertex implies that the connector vectors ("the propagators") k_j, cf. Fig 1, fulfill

$$k_j = P - \sum_1^j q_j \quad \text{ie} \quad k_j = k_{j-1} - q_j \tag{2}$$

CCFM introduce the variables $(z_j, \vec{q}_{\perp j})$ such that $k_{+j} = z_j k_{+(j-1)}$ and $\vec{k}_{\perp j} = \vec{k}_{\perp(j-1)} - \vec{q}_{\perp j}$. In the Leading Log Approximation (LLA), relevant for the CCFM model calculations, the fractional variables should fulfill $z_j \ll 1$, i.e. the splitting functions are approximated by $P(z) \sim 1/z$. While the emitted gluons along the fan diagram in Fig 1 are treated as mass less, the connector vectors k_j are space like with $-k_j^2 \simeq \vec{k}_{\perp j}^2$. This relation is satisfied provided

$$k_{\perp j}^2 > z_j q_{\perp j}^2 \tag{3}$$

while smaller $k_\perp$-values are suppressed. Then the weight and the form factor in Eq (1) is in the CCFM model

$$\bar{\alpha} \frac{dz}{z} \frac{dq_\perp^2}{q_\perp^2} \Delta_{ne}(z, k_\perp, q_\perp) \tag{4}$$

with the effective coupling $\bar{\alpha} = 3\alpha_s/\pi$ and the non-eikonal form factor

$$\Delta_{ne} = \exp(-\bar{\alpha} \ln(1/z) \ln(k_\perp^2 / z q_\perp^2)) \tag{5}$$

The LDC model choice in Ref [1] is to restrict the ISB emissions in the CCFM model to those which also fulfill

$$q_{\perp j} \geq \min(k_{\perp j}, k_{\perp(j-1)}) \tag{6}$$

Gluons which do not satisfy this constraint can be included in the FSB set causing only small recoils. If the ISB set is restricted in this way, and we sum over the corresponding weights and form factors it is in Ref [1] shown that we obtain *the same weight as in Eq (4) but with the non-eikonal factor exchanged for* 1. This is obviously a major simplification in order to calculate the cross sections according to Eq (1).

The second simplification comes with respect to the emission of the FSB radiation. *The FSB gluons are emitted as dipole radiation with the "original" dipoles spanned between the color-adjacent ISB gluons* (q_j, q_{j+1}) *and with the*

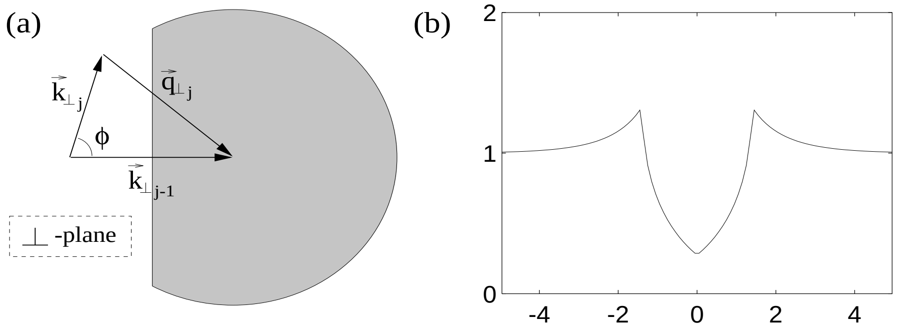

Figure 2: (a) The shaded area denotes the forbidden region for $\vec{k}_{\perp j}$ where $q_\perp < \min(\mathrm{k}_{\perp \mathrm{j}}, \mathrm{k}_{\perp \mathrm{j}-1})$. For $0.5 < k_{\perp j}/k_{\perp j-1} < 2$, the ϕ-integral is limited to a restricted region. (b) The azimuthal average h as a function of $\ln(k^2_{\perp j}/k^2_{\perp (j-1)})$.

largest allowed FSB transverse momentum determined by the propagator virtuality $-k_j^2 \simeq k^2_{\perp j}$. This means that we may for the FSB radiation make use of the well-known Lund Dipole Cascade model [8], as it is implemented in the Monte Carlo simulation program ARIADNE, [9].

The transverse momentum restrictions for the FSB emissions, i.e. that the allowed FSB transverse momentum is limited by the propagator $-k_j^2 \simeq k^2_{\perp j}$, occur also in the CCFM model and is a major result from their very complicated calculations, [2]. Physically it means that the two color adjacent gluon currents from the "dipole pair" (q_j, q_{j+1}) in the LDC model do not stem from the same space-time point. There is a distance, which due to Lorenz contraction is essentially transverse, $b_\perp \sim 1/\sqrt{-k_j^2}$. The constraint then stems from the difficulty to emit FSB radiation with a wave-length $\lambda \simeq 1/q_\perp < b$, i.e. smaller than the "antenna size". In other words there should be a form factor, which if it is e.g. an inverse power in $k_\perp$ is exponentially falling in the relevant $\ln(k_\perp^2)$-variable and therefore leads to negligible contributions to the LLA outside this region.

After azimuthal (ϕ) averaging for fixed $|\vec{k}_{\perp j-1}|$ and $|\vec{k}_{\perp j}|$ over the transverse pole in $\vec{q}^{\,2}_{\perp j} = (\vec{k}_{\perp j} - \vec{k}_{\perp (j-1)})^2$ we obtain with the constraint in Eq (6) (see Fig 2a) the LDC weights

$$\begin{aligned} dw(LDC) &= \bar{\alpha}\frac{dz_j}{z_j}\int \frac{d\phi\, dk^2_{\perp j}}{4\pi \vec{q}^{\,2}_{\perp j}}\theta\left(q_{\perp j} - \min\left(k_{\perp j}, k_{\perp (j-1)}\right)\right) \\ &= \bar{\alpha}\frac{dz_j}{z_j}\frac{dk^2_{\perp j}}{\max(k^2_{\perp j}, k^2_{\perp (j-1)})} h(k^2_{\perp j}/k^2_{\perp (j-1)}) \end{aligned} \tag{7}$$

The function $h(a)$, which is obtained from the azimuthal integration, is given by (see Fig 2b)

$$h(a) = \frac{\left(1 - \frac{2}{\pi}\arctan\left(\frac{1+\sqrt{a}}{1-\sqrt{a}}\sqrt{\frac{2\sqrt{a}-1}{2\sqrt{a}+1}}\right)\theta(a - 1/4)\right)}{1-a}; \quad 0 < a < 1$$

$$h(a) \quad = \quad h(1/a) \tag{8}$$

As $dz_j/z_j = dy_j$, with y_j equal to the rapidity, we see that the expression in Eq. (7) is *completely symmetric, and the chain could equally well be generated from the probe end towards the target.* We also note that in the LLA in general $\ln(k_{\perp j}^2/k_{\perp(j-1)}^2)$ is not close to 0 and then $h(a) \simeq 1$ (although we note that "at the pole" there is a dip $h(1) = \sqrt{3}/2\pi \simeq 0.28$). Thus in the LLA approximation (using $\kappa = \ln(k_\perp^2)$ and $\ell = \ln(1/z)$)

$$dw(LDC) \simeq \begin{cases} \bar{\alpha} d\ell_j d\kappa_j & \text{if } \kappa_j > \kappa_{j-1} \\ \bar{\alpha} d\ell_j d\kappa_j \exp(\kappa_j - \kappa_{j-1}) & \text{otherwise} \end{cases} \tag{9}$$

Therefore we obtain in the LDC model from Eqs (7) and (9) that *the weight distributions are local* (i.e. we may define a Markovian stochastic process). The locality property in particular implies that the process is simple to implement in a Monte Carlo generation program which simultaneously describes *both the structure functions and the final state properties.* Such a general program [10] is now available and is linked to ARIADNE and JETSET [11].

The above-mentioned symmetry implies that we may use either the fractional variable z_{+j} (from the target side) or z_{-j} (from the probe side) as variable in the Monte Carlo generation. In Refs [1] and [3] we have discussed the possibility to extend the scenario outside the LLA. The result is that it is necessary to choose the direction, i.e. to use z_+- or z_--generation, in accordance with the direction of increase in transverse momentum, i.e. in the virtuality, of the propagator. Then the use of the splitting functions in the proper light-cone fraction should contain many of the non-leading contributions to the structure function. The exact results for the radiative corrections are, however, not known in this case. Nevertheless the simplicity and symmetry of the result, i.e. the chain of linked dipoles (containing the FSB and then leading to hadronization in a similar way as in e^+e^--annihilation events) with the restriction of no emission above the corresponding propagator virtuality, seems physically appealing and stable.

In Fig 3 the fan diagram emissions in Fig 1 are described in the well-known Lund dipole phase space (which for any dipole is a triangle in (y, κ) with y the rapidity and with the height and the base-line size given by $\ln(M_{dipole}^2)$). The whole fan emission must occur in between the lines corresponding to $\ln(P_+)$ for the target and $\ln(q_-)$ for the probe (fixed values of the light-cone energy momenta $\ln(k_\pm) = 1/2 \ln(k_\perp^2) \pm y$ correspond to straight lines in the triangle). The emitted gluons are described as extended triangular folds, starting at the (y, κ)-value of the on-shell gluon. The dipoles are spanned between the "tips" of these adjacent gluon folds, i.e. they again correspond to triangles (the two sides of the triangular folds correspond to the colour and anti-colour of the gluon, which are connected each to the two dipoles around the gluon corner). The emission region of each such dipole is limited by the maximum virtuality, which corresponds to the propagator $\ln(-k^2) \simeq \ln(k_\perp^2)$.

A propagator in this plot is specified by a horizontal line indicating its κ-value (transverse momentum) and with the "starting point" (right) given by

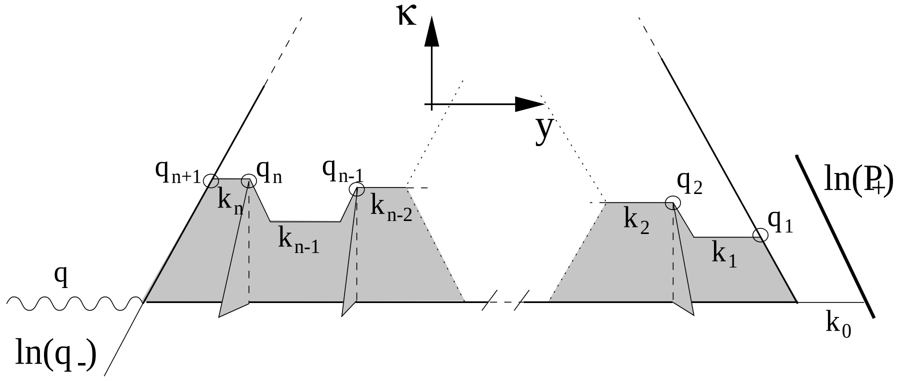

Figure 3: The Dipole phase space in DIS. The shaded area is the phase space for FSB.

the rapidity value $y_- \equiv \ln(-k_\perp/k_-)$ and the "end point" (left) given by $y_+ \equiv \ln(k_+/k_\perp)$. This means that the difference δy between the "endpoint" of one propagator and the "starting point" of the next is

$$0 \leq \delta y = \ln(k_{\perp max}^2) - \ln(k_{\perp min}^2) \tag{10}$$

For completeness we mention that inside the LDC model it is possible, Ref [1], to consider different sub-processes in DIS. Besides the "ordinary" parton model description with Q^2 exceeding all the other momentum transfers in the chains, there is the boson-gluon fusion process, where the the last splitting exceeds Q^2 and all the other ones. Finally in a Rutherford parton scattering process the largest momentum transfer, $k_{\perp max}^2$, will occur somewhere in the middle of the chain. Then we may consider the result of the dipole chain generation as the convolution of the target and the probe structure functions (each developed to the virtuality $-k_{max}^2$ with the Bjorken variables $x_\pm$, respectively) and multiplied by the well-known Rutherford transverse momentum pole $(k_{max}^2)^{-2}$. This also implies that such a Rutherford scattering $k_\perp$ must always be larger than all bremsstrahlung $k_\perp$ in the event. This constraint produces an effective cut-off for small $k_\perp$ Rutherford scattering.

2 The LDC Evolution Equations

2.1 Integral Equations

We study in this paper only purely gluonic chains, and we let the gluonic structure function $F(x, Q^2)$ denote the gluon density in $\ln(1/x)$. (Thus F/x is the density in x.) In this section we will treat the LDC evolution equation for the "non-integrated" structure function, $\mathcal{F}(x, k_\perp^2)$ defined by

$$F(x,Q^2)=\int_{k^2_{\perp cut}}^{Q^2}\frac{dk^2_\perp}{k^2_\perp}\mathcal{F}(x,k^2_\perp)+\int_{Q^2}^{Q^2/x}\frac{dk^2_\perp}{k^2_\perp}\frac{Q^2}{k^2_\perp}\mathcal{F}(x\frac{k^2_\perp}{Q^2},k^2_\perp). \tag{11}$$

Here $k_\perp$ is the transverse momentum of the last link in the chain. We note that the contribution from chains with $k^2_\perp > Q^2$ is suppressed by the factor $Q^2/k^2_\perp$, which makes it sub-leading. We also note the modified argument, $x \to x\cdot k^2_\perp/Q^2$, obtained for this term within the LDC model. Although less important this modification further suppresses this term.

From the weights in Eq (7) we find a recursive relation for $\mathcal{F}$, and in [1] we derived the following evolution equation:

$$\begin{aligned}\frac{\partial\mathcal{F}}{\partial\ell}(\ell,\kappa) &= \int_{\kappa_{cut}}^{\kappa} d\kappa'\bar{\alpha}(\kappa)h(\kappa-\kappa')\mathcal{F}(\ell,\kappa') \\ &+ \int_{\kappa} d\kappa'\bar{\alpha}(\kappa')h(\kappa'-\kappa)\exp[-(\kappa'-\kappa)]\mathcal{F}(\ell+\kappa-\kappa',\kappa')\end{aligned} \tag{12}$$

We have here used the variables $\ell=\ln(1/x)$ and $\kappa=\ln(k^2_\perp)$, introduced in the previous section. The function h defined in Eq (8) originates from the azimuthal integration in Eq (7). From now on we express h in the logarithmic variables κ and κ', and note that it depends only on the difference $|\kappa-\kappa'|$. (Note that in the LLA we can put $h=1$. The argument of $\mathcal{F}$ in the second integral is explained in Eq (10)).

The first integral in Eq (12) corresponds to chains, where the last step is upwards in transverse momentum from κ' to κ, and the second integral, where κ' is larger than κ, to chains with a final step downwards. For the scale in the running coupling we have taken the largest virtuality in each vertex. Thus in the first integral we have $\bar{\alpha}(\kappa)$, while in the second term we have $\bar{\alpha}(\kappa')$.

With a running α_s the result will (as we will see in the following) be rather sensitive to the behaviour in the soft region for small $k_\perp$. Naturally a perturbative calculation cannot be trusted when α_s becomes very large. Lacking a good understanding of the soft region, some kind of cut-off is necessary, and in this paper we have studied the results obtained assuming a lower cut-off, $k_{\perp cut}$ or $\kappa_{cut}=\ln(k^2_{\perp cut}/\Lambda^2)$, in Eqs (11) and (12), while keeping the form $\bar{\alpha}=\alpha_0/\kappa$ for the coupling constant. (Another possibility would be to study the result assuming that α_s saturates for $k_\perp$-values below some cut.)

After a Mellin transform in x_B, which corresponds to a Laplace transform in ℓ with

$$f_\lambda(\kappa)=\int d\ell\exp(-\lambda\ell)\mathcal{F}(\ell,\kappa) \tag{13}$$

we obtain (we will in general neglect the index λ on f from now on)

$$\lambda f(\kappa) = \int^{\kappa} d\kappa' \bar{\alpha}(\kappa) h(\kappa - \kappa') f(\kappa') + \int_{\kappa} d\kappa' \bar{\alpha}(\kappa') h(\kappa' - \kappa) \exp[-(\lambda+1)(\kappa' - \kappa)] f(\kappa') \tag{14}$$

It is sometimes useful (cf section 4) to introduce a symmetric non-integrated structure function $\mathcal{F}_s$ by the definition

$$\mathcal{F}_s(\ell, \kappa) = \mathcal{F}(\ell, \kappa) \exp(-\kappa/2) \tag{15}$$

In that way the exponential suppression factor $\exp -(\kappa' - \kappa)$ in the second integral of Eq (12), which is "paid" only "for going down" in κ, is changed so that "we pay the same amount for going up as for going down" in κ.

2.2 The Case of a Fixed Coupling $\bar{\alpha}$

The case of a fixed coupling has been treated in Ref [1] (and also at many other places) and we will only briefly describe (some of) the results for future reference. We perform a Laplace transform with respect to κ, and define $\hat{f}$ by

$$\hat{f}(\gamma) = \int d\kappa \exp(-\gamma\kappa) f(\kappa) \tag{16}$$

As h is a function of $\kappa - \kappa'$, we actually work with a convolution integral, and pole-singularities are obtained in $\hat{f}$ at the γ-values (the "anomalous dimensions" for given λ) which satisfy

$$\lambda = \bar{\alpha}[g(\gamma) + g(\lambda + 1 - \gamma)] \quad \text{with} \quad g(\gamma) = \int_0^{\infty} d\Delta \exp(-\gamma\Delta) h(\Delta) \tag{17}$$

The two g-contributions stem from the two integrals in Eq (14), respectively. and $h(\Delta)$ is here interpreted as a function of the logarithmic variable $\Delta = \kappa - \kappa'$.

There are different levels of approximations possible to apply in the treatment of the Eqs (12), (14) and (17). The simplest one is to make use of the approximation in Eq (9) and to replace h by 1, which gives $g \approx 1/\gamma$. The function h deviates from 1 around the singular point $\ln(\kappa_j^2/\kappa_{j-1}^2) = 0$, and in an improved treatment we can describe this deviation by a δ-subtraction (cf ref [1]):

$$h \simeq \hat{h} = [1 - A\delta(\kappa - \kappa')] \tag{18}$$

Inserted into Eq (17) this gives

$$g(\gamma) \simeq \bar{\alpha}\,[1/\gamma - A/2] \Rightarrow \lambda \simeq \bar{\alpha}\,[\frac{1}{\gamma} + \frac{1}{\lambda + 1 - \gamma} - A] \tag{19}$$

If we fix A by the condition $\int(\hat{h}(\Delta)-1)d\Delta = \int(h(\Delta)-1)d\Delta$ we find $A \approx 0.65$. In g also other moments of h are important, and in ref [1] it was found that for $A \approx 0.8$ the same λ-value was obtained from the original h and the approximation $\hat{h}$.

We note that the BFKL result corresponds to a neglect of the λ-dependence in the second g-term in Eq (17). Although this is a sub-leading term, it is numerically not small, as discussed in Ref [1]. (There is also in BFKL a different method to regularize the singularity at $\ln(\kappa_j/\kappa_{j-1}) \sim 0$.)

In [1] we also pointed out another important non-leading effect. For consistency it is necessary that "the steps" in $\ln(1/z)$ really are large, but it turns out that there are essential contributions to the BFKL-integrals from eg $z > 1/2$. We return to this problem in section 3.2.

The x_B-dependence is then determined by the inverse Mellin (or Laplace) transform. The leading behaviour stems from a pinch singularity at $\lambda = \lambda_s$, when the two symmetrical solutions to Eq (17) coincide, i.e. when $\gamma = (1+\lambda_s)/2$ (or $\gamma = 1/2$ if the λ-dependence in $g(\lambda+1-\gamma)$ is neglected.) From Eq (19) we find e.g. for $\bar{\alpha} = 0.2$ and $A = 0.8$ the result $\lambda_s \approx 0.41$ (neglecting the λ-dependence in g, we would instead obtain $\lambda_s \approx 0.64$), with the corresponding low-x_B behaviour $\sim x_B^{-\lambda_s}$.

When the inverse Laplace(Mellin)-transform is performed one also obtains the dependence on $k_\perp$ (or rather on $\kappa = \ln(k_\perp^2)$) by a saddle-point approximation around the pinch singularity. The result (besides essentially trivial kinematic factors) is a Gaussian in κ with a width $\sim\sqrt{\ln(1/x)}$, a result which can be interpreted as a kind of random walk in κ-space [5].

2.3 The Case of a Running Coupling $\bar{\alpha}$

For a running coupling, chains with larger κ-values are disfavoured by the smallness of α_s. This will imply that $<\kappa>$ does not increase beyond any bound as in the case with a fixed coupling. Instead the κ-distribution saturates, and for small x, $\mathcal{F}(x, k_\perp^2)$ approaches asymptotically a factorizing form

$$\mathcal{F}(x,\kappa) = x^{-\lambda} f(\kappa). \tag{20}$$

The result appears to be similar to the type of random walk an atmospheric molecule follows in the earth's gravitational field. In this case, when the molecules are constantly pulled downwards, an equilibrium is obtained for an exponentially decreasing density (see also the discussion in Appendix C). As discussed in section 3.3, also in our model with a running α_s the asymptotic $k_\perp$-distribution is an exponential in $\kappa = \ln k_\perp^2$. Inserting the asymptotic form in Eq (20) into Eq (12) implies that $f(\kappa)$ must satisfy Eq (14) above, now with $\bar{\alpha}(\kappa) = \alpha_0/\kappa$, where $\alpha_0 = 12/11$ if we study a purely gluonic situation with no quarks. The solution to this equation will be studied in the following section.

3 The Solution for Running Coupling

We have not been able to find an exact analytic solution to the integral equation (14). Instead we have solved it numerically, using Chebyshev polynomials to convert it to a matrix equation. This method was also used in ref [12], and is discussed further in appendix A. The x-dependence for small x-values is determined by the largest eigenvalue λ to this matrix equation.

In order to better understand the properties of the model we have also studied a set of approximations, which all agree with the original Eq (14) to leading logarithmic accuracy:

a) by using κ instead of κ' for the argument of $\bar{\alpha}$ in the second integral of Eq (14)

b) by using the approximation $h \approx (1 - A\delta(\kappa - \kappa'))$ in Eq (18). A special case (called b') with $A = 0$ corresponds to $h \to 1$.

c) with both of the approximations a) and b) (cf section 3.1). (Case c') corresponds to both approximations a) and b').)

The cases b') and c) can be studied analytically. Case b') is discussed in appendix B, and the simpler case c) will be discussed in section 3.1.

3.1 Qualitative properties

In order to understand the qualitative features of Eq (14) we start by investigating the approximation called c) above, which is obtained when $\bar{\alpha}(\kappa')$ is replaced by $\bar{\alpha}(\kappa)$ in the last integral of Eq (14), and the variation of h is approximated by a δ-function according to Eq (18). We note that both these approximations are of non-leading order, and the solution has properties similar to the solution of the original Eq (14). With these approximations the integral equation in Eq (14) can be transformed by straightforward differentiations into the second-order differential equation

$$u\frac{d^2 f}{du^2} = [(\lambda+1)u - 2]\frac{df}{du} + (\lambda+1)(1-\mu)f \tag{21}$$

where $u = \kappa + \mu A$ and $\mu = \alpha_0/\lambda$. This is equivalent to (the radial part of) the Schroedinger equation for the hydrogen atom with the angular momentum variable $\ell = 0$. To see that, we introduce the function ψ defined by

$$f = \exp[(\lambda+1)/2)u]\psi(u) \tag{22}$$

We obtain by straightforward calculations

$$-\frac{1}{2}\frac{d^2(u\psi)}{udu^2} - \frac{\mu(\lambda+1)\psi}{2u} = -\frac{(\lambda+1)^2\psi}{8} \tag{23}$$

Thus the "mass"-value is unity and the (squared) "charge" equal to $\mu(\lambda+1)/2$.

For large values of κ (large values of u) the second term in Eq (23) can be neglected, and the solution behaves as $u\psi \sim \exp[\pm(1+\lambda)\kappa/2]$. Here the physical solution must correspond to the minus sign. From Eq (22) this implies that f varies as a power of κ for large κ-values. From the behaviour of eq. (21) for large u, ie large κ, we find

$$f \propto \kappa^{\frac{\alpha_0}{\lambda}-1}; \quad \kappa \text{ large} \tag{24}$$

The value of λ is determined by the boundary condition for small κ, which can be derived from the integral equation (14). (With the present approximation we find $f'(\kappa_{cut}) = [1+\lambda - 1/(\kappa_{cut}+\mu A)]f(\kappa_{cut})$.) This implies that we have solutions for a discrete set of eigenvalues λ. The asymptotic behaviour of the solution is determined by the largest of these eigenvalues, which corresponds to a solution ψ with no zeros between κ_{cut} and ∞.

We note that since λ is fixed by the boundary condition, the result is sensitive to the value of κ_{cut}, i e it is sensitive to the soft region. When κ_{cut} increases, the value of λ decreases continuously. Note, however, that if we include the correction term in h then this sensitivity to κ_{cut} is strongly reduced. As $\kappa = \kappa_{cut}$ implies $u_{cut} = \kappa_{cut} + \mu A$ we keep away from the singular point $u = 0$ in Eq (23), even when κ_{cut} approaches 0. This stabilizing effect of h will be further discussed in the following subsection.

For a *fixed* coupling we can from Eq (14) derive a differential equation similar to Eq (21). This equation does not, however, contain the factors u in front of d^2f/du^2 and df/du. Therefore this equation has two exponentially growing solutions, which implies that in this case the dependence of $\mathcal{F}$ upon x and κ does not factorize.

Summarizing we have found that the asymptotic behaviour of $\mathcal{F}$ is given by the form

$$\mathcal{F} \propto x^{-\lambda} \cdot \kappa^{\frac{\alpha_0}{\lambda}-1} \equiv x^{-\lambda} \cdot (\ln k_\perp^2)^{\frac{\alpha_0}{\lambda}-1}; \quad \ln(1/x) \gg \kappa \gg 1 \tag{25}$$

where the power λ is an eigenvalue determined by the boundary conditions. It turns out that these qualitative features do not rely on the approximations used in this subsection, but are also relevant for the solution to the original equation (14).

3.2 The x-dependence

We will now study the numerical solution to Eq (14). As the second integral is sub-leading, we see that for $\bar{\alpha} = \alpha_0/\kappa$ the eigenvalue λ will to first approximation be proportional to α_0. Since we are here studying only purely gluonic chains, and are not including quark links, it may be most consistent to use a value of α_0 which corresponds to a pure Yang-Mills theory. From the relation $\alpha_0 = 36/(33-2n_f)$ we find for a pure Yang-Mills $\alpha_0 = 12/11$ as compared to e.g. $\alpha_0 = 4/3$ for $n_f = 3$.

As we have not studied the influence from the quarks we present results for the more stable quantity λ/α_0. Thus in Fig (4) we show how λ/α_0 depends on

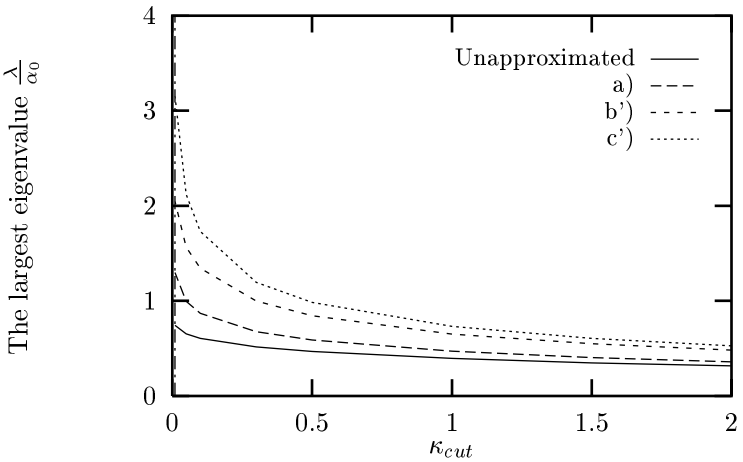

Figure 4: The dependence of λ/α_0 on κ_{cut}. The solid line is from eq. (14) without approximations. The other lines are for the approximations a, b' and c' from down and up. As the calculations do not include quarks we have presented results for the more stable ratio λ/α_0, where $\alpha_0 = 12/11$ for $n_f = 0$ and $\alpha_0 = 4/3$ for $n_f = 3$.

the value of κ_{cut} in the range $0.01 < \kappa_{cut} < 2$ (To be exact the results presented correspond to $\alpha_0 = 12/11$ and for $\alpha_0 = 4/3$ they are about 4% smaller). Results are presented for the original equation (14) and also for the approximations a), b') and c') defined above. We see that the result is sensitive to both the soft cut-off, κ_{cut}, and to the non-leading modifications in the different approximations. We note, however, that the factor h in the LDC model provides a very strong stabilizing effect. Thus for the original non-approximated equation, the result is fairly stable in a range $0.5 < \kappa_{cut} < 2.0$, which ought to contain realistic values for κ_{cut}. In this range we find $0.3\,\alpha_0 < \lambda < 0.5\,\alpha_0$.

In the LLA the energy fractions z_i are assumed to be small compared to 1, and in ref [1] we pointed out that quantitatively significant contributions arise from large z-values. We here show that this is true also with a running coupling. For the splitting function, we have in the weights in Eq (7) used $P(z) \propto 1/z$, which is correct within the leading log approximation. The full splitting function without regularization for $z = 1$ reads

$$P(z) = 2N_c \left\{ \frac{1-z}{z} + \frac{z}{1-z} + z(1-z) \right\} \tag{26}$$

If inserted in an evolution equation, the pole at $z = 1$ has to be regularized. Virtual corrections imply that this pole does not contribute to the increase of the cross section (ie the structure functions) for increasing Q^2. One way to interpret this is to note that in the gluon splitting process the "old" gluon disappears and is replaced by two "new" gluons. Thus only one new extra gluon is produced,

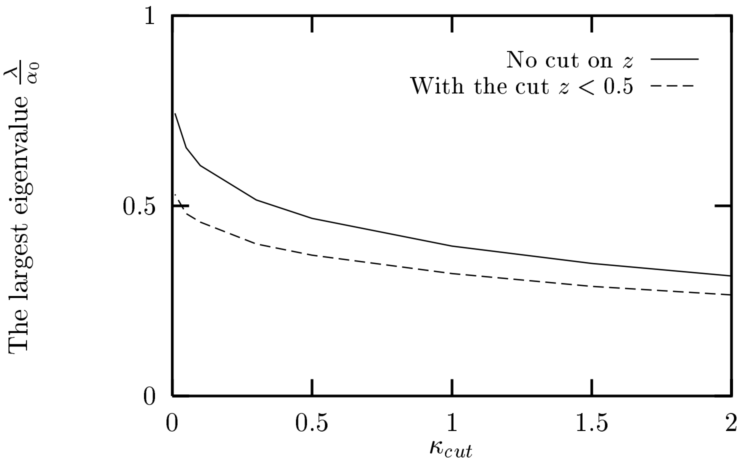

Figure 5: The dependence of λ/α_0 on κ_{cut}. The solid line is for the default splitting function. The dashed line is for $P(z > 0.5) = 0$. As in Fig (4) we present results for the more stable ratio λ/α_0.

and values of z close to the pole $1/(1-z)$ corresponds to the original gluon losing some of its energy. Thus this contribution does not increase the cross section, but only "shifts it" to slightly smaller x-values.

In the LLA the energy fraction z, which corresponds to the "new" gluon, is assumed to be small. If we want to reduce recoils as much as possible, we can say that the "new" gluon by definition is the one with least energy, which must imply that $z < 0.5$ (c.f. ref.). Therefore it might be sensible to replace the factor $1/z$ in the weight in Eq (7) by $(1/2N_c)P(z)\theta(0.5-z)$. To get some estimate of this effect we note that $P(z)/2N_c$ is smaller than $1/z$ in most of the region $0 < z < 0.5$. (Actually $P(z)/2N_c - 1/z$ is positive only for $z > 0.43$, and also here it is fairly small.) Therefore to estimate qualitatively the consequence of this non-leading effect, we have studied the changes obtained from the replacement $1/z \to 1/z \cdot \theta(0.5-z)$. It is straightforward to show that this change will give an extra factor 2^λ to the left hand side of Eq (14), which means that λf will be replaced by $2^\lambda \lambda f$. Apparently, this leads to smaller values of λ with an approximate factor $2^{-\lambda} \approx 1/\sqrt{2}$. In Fig 5, we compare $\lambda(\kappa_{cut})$ for the two alternative splitting functions. This non-leading correction is clearly significant, reducing λ by 20-25%.

We have also checked that the largest eigenvalue is well separated from the smaller ones (see Fig 6). Thus for $\kappa_{cut} = 1$ we find for the largest and the second largest eigenvalue the values 0.4 α_0 and 0.2 α_0. Thus for $\ln(1/x) \gtrsim 5$ the non-leading contribution should be supressed by a factor e^{-1} (and for $\ln(1/x) \gtrsim 10$ by a factor e^{-2}).

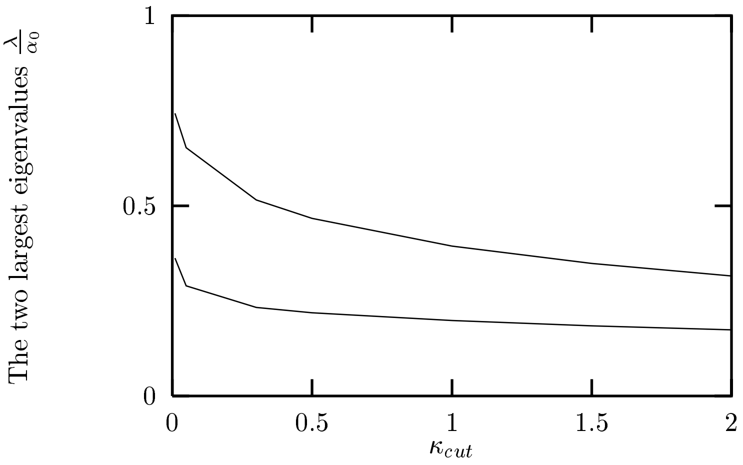

Figure 6: The two largest eigenvalues, as a function of κ_{cut}

3.3 Transverse Momentum Dependence

In Fig 7 we show the solution to the original equation (14) together with approximation b'), which corresponds to the replacement $h \to 1$. It is easy to demonstrate that in all cases $f(\kappa)$ and $\mathcal{F}$ have asymptotically the same powerlike behaviour as the simpler approximation studied in section 3.1, Eqs (24) and (25).

We note, however, that the parameter λ takes on different values in the different approximations. If we calculate the first correction term to f in an expansion in $1/\kappa$

$$f(\kappa) \propto \kappa^{\frac{\alpha_0}{\lambda}-1}\left(1 + b\kappa^{-1} + \mathcal{O}(\kappa^{-2})\right) \tag{27}$$

we obtain

$$b = -\frac{\alpha_0(\alpha_0-\lambda)}{\lambda}\left[\frac{1}{1+\lambda} - \mathcal{A}\right] \quad \text{where} \quad \mathcal{A} = \int (1-h(\Delta))d\Delta \approx 0.65 \tag{28}$$

For $\lambda \approx 0.4$, b is very small, and from Fig 7 we see that the single power in Eq (24) is a surprisingly good approximation in the whole κ-range. (For the approximation b') with $h \to 1$, we have $\mathcal{A} = 0$, and the correction term becomes much larger, as is also seen in Fig 7.)

We note that the powerlike dependence on κ for f and $\mathcal{F}$ implies a similar power dependence also for the original "integrated" structure function F. For small x we have from Eqs (20) and (11)

$$\begin{aligned} F &= x^{-\lambda}\tilde{F}(\ln Q^2) \\ \tilde{F} = \int_{\kappa_{cut}}^{\ln(Q^2)} f(\kappa)d\kappa &+ \int_{\ln(Q^2)} e^{(1+\lambda)(\ln(Q^2)-\kappa)} f(\kappa)d\kappa \end{aligned} \tag{29}$$

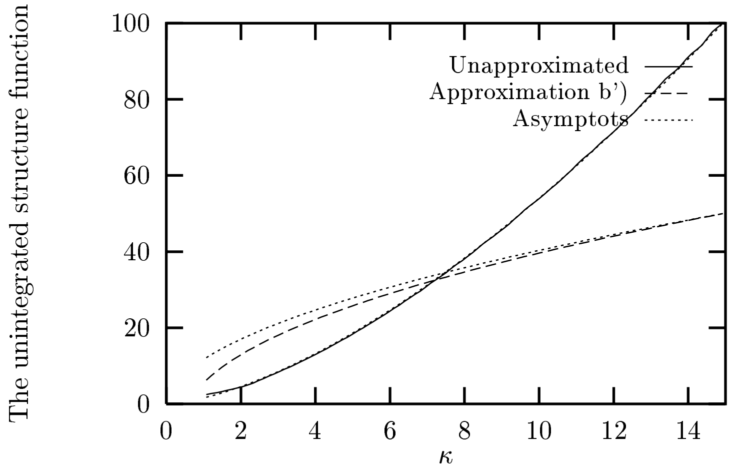

Figure 7: The solution $f(\kappa)$ to the integral eqaution (14) (solid line) and for the approximation b') (dashed line) together with the asymptotic forms.

The result is presented in Fig 8, which also shows the separate contributions in Eq (29). These contributions correspond to chains with $k_\perp^2 < Q^2$ and $k_\perp^2 > Q^2$ respectively, where $k_\perp$ is the transverse momentum of the last link in the chain.

Inserting the asymptotic expression in Eq (27) we find for large Q^2

$$F \propto x^{-\lambda}(\ln Q^2)^{\alpha_0/\lambda}; \;\; \ln(1/x) \gg \ln(Q^2) \gg 1 \tag{30}$$

For large Q^2 the first integral in eq (29) dominates, and for this term the single power in Eq (30) is a good approximation. The second integral is suppressed by the factor $\frac{\alpha_0}{\lambda(1+\lambda)} \cdot \frac{1}{\kappa}$, which for $\ln Q^2 = 10$ is about 20% , but becomes relatively more important for smaller Q^2. Thus, if we use the power expansion of f in Eq (27), we get for $b \approx 0$ the better estimate

$$\tilde{F} \propto (\ln Q^2)^{\frac{\alpha_0}{\lambda}} \left[1 + \frac{\alpha_0}{\lambda(1+\lambda)} \cdot \frac{1}{\ln Q^2} + \mathcal{O}\left((\ln Q^2)^{-2}\right)\right] \tag{31}$$

To better illustrate the $k_\perp$-dependence of the chain, we have studied a very long chain in order to find out where this chain passes the central line $y = 0$. It is straight forward to show that the density ρ (in the (y,κ)-plane) of all the right hand endpoints of the horizontal lines in the diagram in Fig 3, is given by the expression

$$\rho = F(\ell_1, \kappa) \cdot \mathcal{F}(\ell_2, \kappa) \cdot \exp(-\kappa) \tag{32}$$

where $\ell_1 = \ln W - \kappa/2 + y$, $\ell_2 = \ln W - \kappa/2 - y$ and W equals the total cms energy of the chain. The non-integrated function $\mathcal{F}(\ell_2, \kappa)$ describes the weight for the chains coming from left in Fig 3 to the point (y, κ), while the normal structure function $F(\ell_1, \kappa)$ adds up the contributions from links with all possible

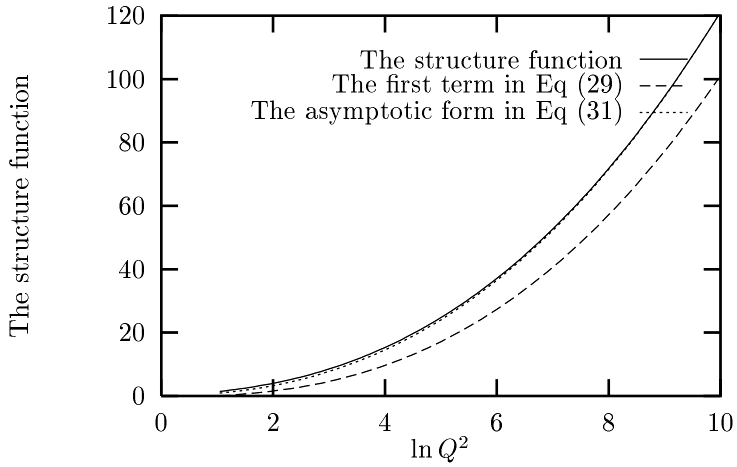

Figure 8: The $\ln Q^2$-dependence of the structure function. The dashed line is the contribution from the first term in Eq. (29). The dotted line is the contribution from the two first terms in the power expansion in Eq (31).

values of κ', both those larger than κ and those smaller than κ. Inserting the asymptotic expressions in Eqs (25) and (30) we find the following result (the factor $\exp(-\lambda\kappa)$ comes from the κ-dependences of ℓ_1 and ℓ_2)

$$\rho \sim \kappa^{\frac{2\alpha_0}{\lambda}-1} e^{-(1+\lambda)\kappa}; \;\; W \text{ and } \kappa \;\text{ large} \tag{33}$$

In Fig 9 we present the results from a Monte Carlo simulation for different energies W of the quantity ρ in Eq (32). We note that the distribution has the expected approximate exponential fall off $\sim \exp[-(1+\lambda)\kappa]$, in accordance with Eq (33) and this corresponds to a (negative) power dependence in $k_\perp$ for the density ρ. Further the curve has the same slope independent of the total energy W, consistent with an asymptotically factorizing dependence on x and $k_\perp$, i.e. there is no sign of the expected BFKL diffusion in κ. The dashed line in Fig 9 shows the asymptotic form in Eq (33).

For comparison we also show in Fig 9 the result for a constant coupling $\bar{\alpha} = 0.2$. Here we find a Gaussian distribution with a width increasing with the energy ($\sim \sqrt{\ln 1/x}$), as expected from a random walk.

4 Dominating Paths in Transverse Momentum

The result in Eq (30) is particularly interesting if we compare to a result obtained in [3], where we study the mean paths of the initial state cascade in the (ℓ, κ)-plane. We find that due to the running coupling the region covered by the major contributions (nowadays known as the "Bartel cigar") corresponds to one part, length ℓ_1, with small κ-values and with a BFKL-like contribution,

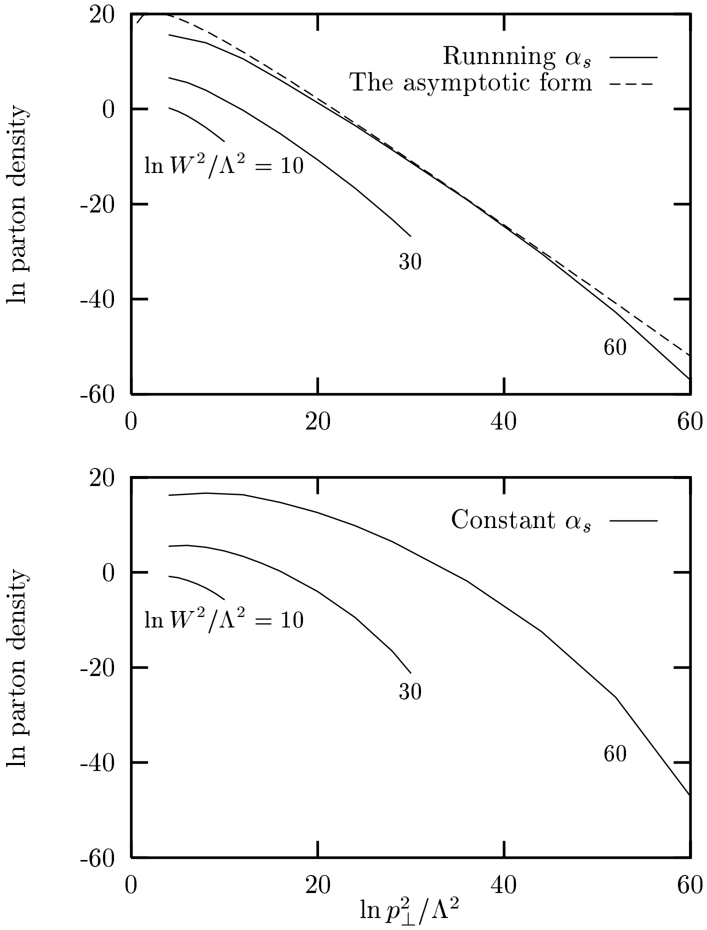

Figure 9: Transverse momentum distributions in the centre of a long chain for different values of hadronic central mass W for running vs. fixed α_s.

$\simeq$exp($\lambda\ell_1$) and a second part, length $\ell_2 = \ell - \ell_1$, corresponding to increasing κ-values up to the final $\kappa_Q \equiv \ln(Q^2)$. This second part is a DGLAP contribution, $\simeq$exp($2\sqrt{\alpha_0 \ell_2 \chi_Q}$), where $\chi_Q = \ln(\kappa_Q)$. Using a saddle-point approximation we demonstrated that the combination of the two parts corresponds for $\lambda\ell > \alpha_0\chi_Q/\lambda$ to

$$\mathcal{F} \sim \exp(\lambda\ell + \alpha_0\chi_Q/\lambda) \tag{34}$$

which is identical to our result from Eq (30).

For $\lambda\ell < \alpha_0\chi_Q/\lambda$ the DGLAP chains dominate, because in this case the saddle-point is not within the the allowed integration region. We note that this result implies that the BFKL behaviour is relevant only for rather small x-values, $x \sim 10^{-5}$ for $Q^2 \sim 100$ GeV^2.

We will end by showing that for small x-values the very construction of the LDC chains leads to a simple result of the BFKL kind. In the LDC model it is possible to go "up" and "down" in κ along the chains, and thus the total chain can be divided into "cells", where each cell contains a set of up-steps followed by another set of down-steps. Let us study one such cell, which starts in the point at (y_1, κ_1), goes up to a maximum point (y', κ'), and then goes down to the endpoint (y_2, κ_2). We note that this second part corresponds to up-steps from the probe side, and therefore both pieces correspond to "DGLAP-chains".

To describe the path we generalize the structure function $\mathcal{F}$ to a function $\mathcal{F}(\ell, \kappa_2, \kappa_1)$, which describes the sum of all paths, which start at a virtuality given by κ_1 (which may now be different from κ_{cut}) and end at κ_2. It is also convenient to include the exponential factor in Eq (32) into the structure function, and define a "symmetrized structure function" $\mathcal{F}_s$ by the relation

$$\mathcal{F}_s(\ell, \kappa_2, \kappa_1) = e^{-(\kappa_2 - \kappa_1)/2}\mathcal{F} \tag{35}$$

If expressed in the rapidity separation between the two endpoints, $\delta y = \ell + (\kappa_2 - \kappa_1)/2$, this function is fully symmetric with respect to the direction of the chain. The result for a long chain is also the direct product of the separate pieces.

Inserting the DGLAP-result for the two sections in the cell, and integrating over possible intermediate points (y', κ') we find

$$\begin{aligned}
&\mathcal{F}_{s,cell}(\delta y = y_2 - y_1, \kappa_2, \kappa_1) \\
&\approx e^{-(\kappa_2-\kappa_1)/2} \int d\kappa' dy' e^{-(\kappa'-\kappa)} \mathcal{F}_{DGLAP}(\ell_1, \kappa', \kappa_1)\mathcal{F}_{DGLAP}(\ell_2, \kappa', \kappa_2) \\
&where\ \ \ell_1 = y' - y_1 - (\kappa' - \kappa_1)/2; \ \ \ell_2 = y - y' - (\kappa' - \kappa_2)/2
\end{aligned} \tag{36}$$

We start by considering the simpler case with a fixed coupling $\bar{\alpha}$, for which we have

$$\mathcal{F}_{DGLAP}(\ell, \kappa', \kappa_1) \simeq exp(2\sqrt{\bar{\alpha}\ell(\kappa' - \kappa_1)}) \tag{37}$$

Inserted into Eq (36) this gives

$$\mathcal{F}_{s,cell} \approx \int dy' d\kappa' \exp[2\sqrt{\bar{\alpha}\ell_1(\kappa'-\kappa_1)} + 2\sqrt{\bar{\alpha}\ell_2(\kappa'-\kappa_2)} - \kappa' + \kappa_2/2 + \kappa_1/2] \quad (38)$$

where ℓ_1 and ℓ_2 are given by Eq (36). This integral can be solved by stationary-phase methods, i.e. we look for the saddle-point in the integrand exponent. After a little algebra we find the surprisingly simple result that

$$\mathcal{F}_{s,cell} \simeq \exp[(R-1)\delta y/2] \quad \text{with} \quad R = \sqrt{1+8\bar{\alpha}} \text{ and } \delta y = y_2 - y_1 \quad (39)$$

Thus the contribution from one cell depends only upon the rapidity difference between the starting point and the endpoint. This also means that this result can be easily generalized to any number of cells.

A closer examination tells us, however, that the maximum is only obtained within the integration region if δy is large compared to $\delta\kappa = \kappa_2 - \kappa_1$. There will be a dividing line with

$$\delta\kappa = \frac{R-1}{R}\delta y \quad (40)$$

(where R is defined in Eq (39)) with the property that for smaller κ-values there is a saddle-point but for larger κ the main contribution is a single DGLAP-motion always directed upwards in κ. For κ below the line the result is obviously of the BFKL kind, i.e. there is (besides the symmetrical κ-dependence) an effective $x^{-\lambda_e}$ behaviour, but this time with $\lambda_e = (R-1)/2 \simeq 0.3$ for our "conventional" value of $\bar{\alpha} \simeq 3/\pi \times 0.2$.

For a running coupling, cells which go very high up in κ are suppressed. Therefore the cells will have limited sizes, both in κ and in y, and for very small x the number of cells will be proportional to the total rapidity range, $\ln(1/x)$. The result becomes a BFKL-like power-dependence on $1/x$ but a saturating distribution in κ, which is described by the limited κ-distribution in a single cell, a behaviour which is in agreement with our results in section 3. The dividing line in Eq (40) will be relevant in the region not too far from the target end, before the κ-distribution saturates for very large rapidity separations.

5 Conclusions

We have shown that if we introduce a running coupling $\bar{\alpha} = \alpha_0/\kappa$ into the integral equations for the gluon structure function in the LDC model then

- for the non-integrated structure function $\mathcal{F}(\ell \equiv \ln(1/x), \kappa \equiv \ln(k_\perp^2))$ we obtain a factorizing BFKL-like behaviour

$$\mathcal{F}(\ell,\kappa) \simeq \exp(\lambda_m \ell) f_{\lambda_m}(\kappa) \quad (41)$$

  where the largest eigenvalue λ_m is isolated. It depends upon the soft cutoff κ_c but takes on stable values $\lambda_m \simeq 0.4\,\alpha_0$ for $0.5 \leq \kappa_c \leq 2$. Further a very good approximation for f_{λ_m} valid for $\kappa > \kappa_c$ is

$$f_{\lambda_m} \simeq \kappa^{\alpha_0/\lambda_m - 1} \quad (42)$$

- For the (integrated) structure function $F(\ell \equiv \ln(1/x), \kappa_Q \equiv \ln(Q^2))$ we then obtain, again as a good approximation for large ℓ, $(\lambda_m \ell > \alpha_0 \ln(\kappa_Q)/\lambda_m)$

$$F(\ell, \kappa_Q) \sim const \cdot \exp(\lambda_m \ell + \alpha_0 \ln(\kappa_Q)/\lambda_m) \tag{43}$$

which, as it is demonstrated in [3], corresponds to an interpolation between the BFKL and DGLAP mechanisms. For $\alpha_0 \ln(\kappa_Q)/\lambda_m > \lambda_m \ell$ the DGLAP mechanism dominates and there is evidently according to Eq (43) a smooth turnover to DGLAP when $\alpha_0 \ln(\kappa_Q)/\lambda_m = \lambda_m \ell$.

- The expected BFKL-diffusion in κ (with ℓ as the "time"-variable) is not noticeable in the model. For large values of ℓ we obtain in the center of phase space a saturating κ-distribution (valid at least for $\kappa > 2$)

$$\rho d\kappa \simeq d\kappa \kappa^{2\alpha_0/\lambda_m - 1} \exp\left[-(\lambda_m + 1)\kappa\right] \simeq \frac{dk_\perp^2}{k_\perp^{4+2\lambda_m}} \bar{\alpha} \cdot (\ln(k_\perp^2))^{2\alpha_0/\lambda_m} \tag{44}$$

which may be characterized as a kind of "renormalized Rutherford cross section".

A Numerical Method for Solving the Integral Equation

We will here briefly describe the method of using Chebyshev polynomials for solving the integral equation (14).

The Chebyshev polynomials are defined by

$$T_n(x) = \cos n(\arccos x), -1 < x < 1$$

and obey the orthogonality relation

$$\int_{-1}^{1} \frac{T_m(x)T_n(x)}{\sqrt{1-x^2}} = \begin{cases} 0, m \neq n \\ \frac{\pi}{2}, m = n \neq 0 \\ \pi, m = n = 0 \end{cases} \tag{45}$$

The eigenfunction and the kernel of the integral equation (times a factor $\sqrt{1-x'^2}$, because of the weight factor in the orthogonality relation) are expanded in Chebyshev polynomials, up to a certain degree N, thus converting the integral equation to an approximately equivalent matrix equation. Usually, we are interested in the largest eigenvalue and the corresponding eigenfunction.

For practical reasons, we must approximate the upper limit in the integral equation with a large number which we have set to $\kappa_{max} = 100$. No significant dependence on the value of $\kappa_{max} > 50$ has been noted.

Normally, the error in the largest eigenvalue λ is less than 1% for the number of polynomials $N > 50$ but we have used up to 320 polynomials to get a good description of the eigenfunctions for large κ-values.

In this work, we have used computer code from Numerical Recipes [13].

B Analytic Solution to the Approximated Integral Equation

In this appendix we will present an analytic solution to the integral equation:

$$\lambda f(\kappa) = \bar{\alpha} \int_{\kappa_{min}}^{\kappa} f(\kappa') d\kappa' + e^{(\lambda+1)\kappa} \int_{\kappa}^{\kappa_{max}} \bar{\alpha} f(\kappa') e^{-(\lambda+1)\kappa'} d\kappa', \qquad (46)$$

with a running coupling $\bar{\alpha}(\kappa) = \alpha_0/\kappa$. This corresponds to approximation b') in section 3.2 where h is replaced by 1.

For finite κ_{min}, κ_{max} the integral equation is solved by rewriting it to a standard differential equation with solutions which are expressed in confluent hyper geometric functions. Using the boundary condition at κ_{max} and taking the limit $\kappa_{max} \to \infty$, we find that solutions to the integral equation have the asymptotic ($\kappa \to \infty$) behaviour $f(\kappa) \sim \kappa^{\frac{\alpha_0}{\lambda}-1}$. Using also the boundary condition at κ_{min}, the largest eigenvalue can be found as a function of κ_{min}. No simple relation for $\lambda(\kappa_{min})$ is found so it is evaluated numerically. The results are in agreement with the numerical solution of the integral equation.

We start by changing variables to $u = (\lambda+1)\kappa$ to get rid of λ from the right hand side of the integral equation (46) which becomes

$$\frac{\lambda}{\alpha_0} \tilde{f}(u) = \frac{1}{u} \int_{u_{min}}^{u} \tilde{f}(u') du' + e^{u} \int_{u}^{u_{max}} \frac{e^{-u'}}{u'} \tilde{f}(u') du'. \qquad (47)$$

This can be rewritten to the differential equation

$$\left(\frac{\tilde{f}' - \tilde{f}}{-\frac{1}{u^2} - \frac{1}{u}} \right)' = \frac{\alpha_0}{\lambda} \tilde{f}. \qquad (48)$$

With

$$y(u) \equiv \frac{\tilde{f}' - \tilde{f}}{-\frac{1}{u^2} - \frac{1}{u}} \Rightarrow f(\kappa) = \tilde{f}(u) = \frac{\lambda}{\alpha_0} y'(u),$$

it can be rewritten to the following differential equation for $y(u)$

$$y'' - y' + \left(\frac{1}{u^2} + \frac{1}{u} \right) \frac{\alpha_0}{\lambda} y = 0. \qquad (49)$$

Two linearly independent solutions are given by the real and imaginary part of the function (see e.g. Ref [14])

$$\tilde{M}(u) \equiv \frac{\Gamma\left(\frac{1}{4} - \nu^2 + i\nu\right)}{\Gamma(1 + i2\nu)} u^{\frac{1}{2}+i\nu} M\left(\frac{1}{4} - \nu^2 + i\nu, 1 + i2\nu; u \right),$$

where $\nu \equiv \sqrt{\frac{\alpha_0}{\lambda} - \frac{1}{4}}$ and M is the standard notation of the confluent hyper geometric function:

$$M(a, b; u) = \sum \frac{a(a+1)\cdots(a+n-1)}{b(b+1)\cdots(b+n-1)} \frac{u^n}{n!}.$$

The real and imaginary parts of $\tilde{M}$ have the asymptotic behaviour

$$\begin{aligned} y_1(u) \equiv \mathrm{Re}\left[\tilde{M}(u)\right] &\sim u^{-\frac{\alpha_0}{\lambda}} e^u \\ y_2(u) \equiv \mathrm{Im}\left[\tilde{M}(u)\right] &\sim u^{\frac{\alpha_0}{\lambda}} \end{aligned} \tag{50}$$

To find the boundary conditions from the integral equation we insert the differential operator in the left hand side of eq. (48) into the integral equation. The boundary conditions are

$$\begin{aligned} \left[\frac{\tilde{f}' - \tilde{f}}{-\frac{1}{u^2} - \frac{1}{u}}\right]_{u=u_{min}} &= 0 \\ \left[e^{-u}\frac{u\tilde{f}' + \tilde{f}}{1+u}\right]_{u=u_{max}} &= 0. \end{aligned} \tag{51}$$

From the second boundary condition, we see that the power solution (y_2 in Eqs. (50)) becomes more and more important as $u_{max} \to \infty$. This means that solutions to the integral equation have the asymptotic behaviour $f(\kappa) \sim \kappa^{\frac{\alpha_0}{\lambda}-1}$.

Having singled out y_2, we use the lower boundary condition, which simply means $y(u_{min}) = 0$, to find a relation between the largest eigenvalue λ and κ_{min}. For each λ, κ_{min} is given by the largest zero of the function $y_2(u)$.

Also in standard notations, the function $y_2(u)$ can be written (apart from a constant factor)

$$y_2(u) = u^{\frac{1}{2}+i\nu} U\left(\frac{1}{4} - \nu^2 + i\nu, 1 + i2\nu; u\right),$$

where U has the following definition:

$$U(a,b;u) \equiv \frac{\pi}{\sin \pi b}\left[\frac{M(a,b;u)}{(a-b)!(b-1)!} - \frac{u^{1-b}M(a+1-b,2-b;u)}{(a-1)!(1-b)!}\right].$$

The solution $y_2(u)$, having a zero at $u = u_{min}$, is equivalent to requiring

$$\mathrm{Arg}\left[\tilde{M}(u_{min})\right] = -n\pi, \tag{52}$$

with n an integer. For very small u_{min} it is sufficient to include the leading term in an expansion of $\tilde{M}$. In this case eq. (52) can be approximated by the relation

$$\ln u_{min} = -\frac{n\pi}{\nu},$$

which means that $n = 1$ is relevant for the largest zero. A less severe approximation (for finite u_{min}) is given by using the first three terms in the expansion of $M(a,b;u)$ and evaluating $\mathrm{Arg}[\tilde{M}(u_{min})]$ numerically. This leads to an approximate relation between κ_{min} and the largest eigenvalue λ, which agrees well with the numerical solution discussed in appendix A.

C Random walk analogy

As mentioned in the main text, for a running coupling constant the chain has similarities with a random walk in a force field. Let us first study a simple example to show what happens if a stochastic process of the Brownian motion type contains a "force". Consider a set of discrete "space-locations" indexed $1, \ldots, j, \ldots$ and assume that at the discrete "times" $t = 1, \ldots, a, \ldots$ there is a number of "objects", $n(t = a, j)$ at the location indexed j. Assume further that there is a rule so that the number of objects changes with time according to

$$n(a+1, j) = \frac{1+\alpha}{2} n(a, j+1) + \frac{1-\alpha}{2} n(a, j-1) \tag{53}$$

Thus there is for a positive α a tendency for the sites with a larger space index to lose to the sites with a smaller index as the time goes by, i.e. the change in the distribution contain a "force" directed towards small space indices.

The equation can (by subtraction of $n(a, j)$ on both sides and a limiting procedure in space x and time t) be rewritten into (the space-size and time-size parameters are d and τ, respectively)

$$\frac{\partial n}{\partial t} = \frac{d^2}{2\tau} \frac{\partial^2 n}{\partial x^2} + \frac{\alpha d}{\tau} \frac{\partial n}{\partial x} \tag{54}$$

For $\alpha = 0$ we obtain the well-known diffusion equation for n, i.e. a Gaussian with an average and a width both increasing with time $\sim \sqrt{t}$. For $\alpha > 0$ we find, however, that starting with a narrow distribution at $t = 0$, the last term in Eq (54) becomes increasingly important when t increases. Thus the time derivative becomes reduced. For $t > \tau/\alpha^2$ the two terms on the right hand side become of equal magnitude in the dominating interval around $x = d\sqrt{t/\tau}$. This implies that the solution approaches the time-independent distribution

$$n \simeq \exp(-\alpha x/d) \tag{55}$$

This is just what happens for e.g. the atmospheric density of the earth.

This example is not totally a relevant one for the BFKL mechanism because the occurring weight distribution has no simple probabilistic interpretation (although positive definite it is non-normalized as the weight corresponds to a density). Nonetheless there are obvious similarities, all weights contain the notion of a "direction", in this case a preferred direction towards small κ-values in the cascade chains because of the running coupling, and the result is asymptotically an exponential distribution in κ.

References

[1] B. Andersson, G. Gustafson, J. Samuelsson, *Nucl. Phys.* **B463** (1996) 217.

[2] M. Ciafaloni, *Nucl. Phys.* **B269** (1988) 49;
S. Catani, F. Fiorani, G. Marchesini, *Phys. Lett.* **B234** (1990) 339, *Nucl. Phys.* **B336** (1990) 18.

[3] B. Andersson, G. Gustafson, H. Kharraziha and J. Samuelsson, *Z. Phys.* **C71** (1996) 613.

[4] E.A. Kuraev, L.N. Lipatov and V.S. Fadin, *Zh. Eksp. Teor. Fiz.* **72** (1977) 373, *Sov. Phys. JETP* **45** (1977) 199;
Ya.Ya. Balitsky and L.N. Lipatov, *Yad. Fiz.* **28** (1978) 1597, *Sov. J. Nucl. Phys.* **28** (1978) 822.

[5] J. Kwiecinski et al.,*Phys. Rev.* **D50** (1995) 217

[6] V.N. Gribov, L.N. Lipatov, *Sov. J. Nucl. Phys.* **15** (1972) 438 and 675;
G. Altarelli, G. Parisi, *Nucl. Phys.* **B126** (1977) 298;
Yu.L. Dokshitzer, *Sov. Phys. JETP* **46** (1977) 641.

[7] Yu.L. Dokshitzer, V.A. Khoze, A.H. Mueller and S.I. Troyan, Basics of Perturbative QCD (Editions Frontiéres, Gif-sur-Yvette, 1991)

[8] G. Gustafson, *Phys. Lett.* **B175** (1986) 453;
G. Gustafson, U. Petterson, *Nucl. Phys.* **B306** (1988) 746;
B. Andersson, G. Gustafson, L. Lönnblad, *Nucl. Phys.* **B339** (1990) 393.

[9] L. Lönnblad, *Comput. Phys. Comm.* **71** (1992) 15.

[10] H. Kharraziha, L. Lönnblad, LU-TP 97-21, H. Kharraziha, L. Lönnblad, LU-TP 97-34

[11] T. Sjöstrand, *Comput. Phys. Comm.* **82** (1994) 74

[12] J. Kwiecinski, A.D. Martin, P.J. Sutton, *Phys. Rev.* **D52** (1995) 1445

[13] W.H. Press, S.A. Teukolsky, W.T. Vetterling and B.P. Flannery, NUMERICAL RECIPES in C *The Art of Scientific Computing* 2:nd ed. (Cambridge University Press).

[14] M. Abramowitz and I.A. Stegun, Handbook of Mathematical Functions (DOVER PUBLICATIONS INC., NEW YORK).